Hindawi
Shock and Vibration
Volume 2024, Article ID 9243316, 14 pages
https://doi.org/10.1155/2024/9243316

Research Article

Shock Reduction Technique in Thin-Plate Structure Using Elastic Patches with Gradual Thickness Variations

Hyun-Su Park,[1] **Dae-Hyun Hwang**,[2] **and Jae-Hung Han**[1]

[1]*Department of Aerospace Engineering, KAIST, Daejeon 34141, Republic of Korea*
[2]*Perigee Aerospace Inc., Daejeon 34141, Republic of Korea*

Correspondence should be addressed to Jae-Hung Han; jaehunghan@kaist.ac.kr

Received 10 November 2023; Revised 6 January 2024; Accepted 16 January 2024; Published 25 January 2024

Academic Editor: Junhong Park

Reducing structural shocks propagated as elastic waves in thin plate-like structures is of paramount importance in diverse engineering applications. In this study, a shock reduction method using elastic patches that deflect bending waves through wave refraction, while maintaining the structural stiffness and strength is presented. Elastic patches with gradual thickness variation were designed and thoroughly investigated both numerically and experimentally. Two types of triangular elastic patches, flat and pyramid-shaped, were utilized to refract and attenuate transient bending waves at different incident angles. All results from ray tracing, finite element analysis, and experiments consistently demonstrated the effective reduction of passing waves in areas behind the attached patches. Moreover, the influence of gradual thickness variation was thoroughly discussed. The proposed method provides a practical approach to mitigate transient shock responses in specific target areas across various structural applications without compromising structural stiffness and strength.

1. Introduction

In order to minimize the dynamic response of structures caused by transient shock loads, numerous researches have been conducted. The objective is to reduce the propagation of shock waves, which behave as elastic waves, and the most commonly employed method is through the utilization of passive shock/vibration isolators [1, 2]. These isolators are specially designed to decrease the transmission of shocks to subsystems, particularly electronic devices. Youn et al. [3] introduced a novel three-axis hybrid mesh isolator that effectively utilizes the pseudoelastic properties of a shape memory alloy (SMA) wire. By taking advantage of the unique characteristics of the SMA wire, the isolator can absorb and dissipate the energy associated with shocks and vibrations, thereby providing protection to the sensitive electronic equipment. Furthermore, Jeong et al. [4, 5] developed a vibration isolator that is capable of actively controlling vibrations in response to dynamic loads. This isolator incorporates an SMA wire actuator, which allows for frequency tunability. Although these isolators exhibit impressive performance in attenuating shocks and vibrations, their precise design and safety testing are crucial due to the potential amplification of low-frequency vibrations near the natural frequency of the system. Additionally, the isolators themselves are susceptible to damage under harsh operating conditions. To address these challenges, the present authors [6] proposed an alternative solution using a Sandwich panel insert.

In addition to shock attenuation, advanced methods have been developed to manipulate the propagation of elastic waves, finding applications in various engineering fields such as vibration filtering, wave guiding, and impact mitigation. Elastic waves vary in propagation speed and characteristics depending on the properties of the medium. Ongoing research aims to mathematically and experimentally investigate wave propagation characteristics in various complex media, ranging from traditional isotropic materials to other complex media, such as transversely isotropic media [7, 8] and infinitely periodic media [9]. The choice of platform for wave manipulation systems is crucial, with microlattice/macrolattice structures arranged periodically

being a common selection [10]. Moreover, extensive research has been conducted on wave manipulation techniques based on metamaterials and phononic crystals. Zhu et al. [11] presented an elastic metamaterial with chiral microstructures that achieves negative refraction of elastic waves. Negative refraction refers to the phenomenon where waves change direction in the opposite sense to that described by Snell's law, which governs the behavior of wave at the interface between different media. In traditional, positive refraction, wave bends towards the normal line drawn at the interface between two materials with different refractive indices. However, in negative refraction, the wave bends away from normal line, resulting in an angle of refraction on the opposite side. Li et al. [12] proposed a scheme for sharply bending acoustic waves by truncating sonic crystals. Huang et al. [13] introduced an elastic metamaterial with a triangular lattice that exhibits near-zero refraction index, allowing for topological zero refraction at arbitrary angles of incidence and across a wide frequency range. Ahn et al. [14] designed an anisotropic elastic metamaterial slab capable of conical refraction for horizontally incident longitudinal or transverse waves. Additionally, Li et al. [15] proposed adaptive metasurfaces composed of arrayed piezoelectric units with individually connected negative capacitance elements that enable modulation of incoming wave fronts of elastic waves through electromechanical tuning. Furthermore, research groups have developed attachment-type metamaterial modules for applications in various structures. Yan et al. [16] conducted a numerical study on bonding a two-dimensional planar array of small lead discs on an aluminum plate with silicone rubber to focus low-frequency flexural guided waves. Tol [17] investigated a phononic crystal Luneburg lens through design, fabrication, and analysis, demonstrating omnidirectional elastic wave focusing and enhanced energy harvesting numerically and experimentally. Also, a 3D-printed phononic crystal lens was developed by Tol for elastic wave focusing and energy harvesting [18]. These gradient refractive index (GRIN) elastic lenses consist of a spatial region where the physical parameters defining the wave velocity vary depending on position. The continuous variation of refractive index required by GRIN devices cannot be achieved with discrete lattice structures, as it would result in a stepped profile. Thus, the unit size must be sufficiently small to ensure a smoother stepped profile. However, this small unit size imposes limitations on the operating frequency.

Recent studies have focused on manipulating elastic waves in thin-plate-like structures to achieve shock reduction or energy harvesting without being limited by frequency constraints. Krylov [19] introduced the concept of the acoustic black hole (ABH) effect, which enables almost perfect absorption of incident wave energy. The fundamental principle behind ABH involves a linear or higher-order power-law decrease in the velocity of the incident wave. The gradual decrease in the speed of wave creates a situation where waves converge towards a central point, similar to how gravity causes matter to converge towards the singularity of a black hole. Most investigations of ABH have focused on bending waves in thin plates. O'Boy and Krylov [20] developed a numerical approach to calculate mobilities for a circular plate with a tapered central hole exhibiting a power-law profile. Subsequently, several research groups have explored various aspects of ABH, including the effects of wedge truncation [21], broadband vibration attenuation characteristics [22], strip ABH indentations [23], and noise reduction across a wide frequency range [24]. The ABH technique demonstrates excellent performance in absorbing wave energy. However, in practical applications, the already thin-plate structure may need to be made even thinner or incorporate cut-out holes, which can result in a reduction of the structural stiffness and strength.

In the pursuit of preserving the structural properties of thin plates, several research groups have explored simple methods. The velocity of waves in a thin plate is influenced by the material properties and plate thickness. The phenomenon of refraction, where waves are bent as they propagate from one medium to another due to differences in propagation velocity, is also observed in bending waves on plates [25, 26]. Based on these characteristics, researchers have focused on designing thickness fields that can achieve effects such as negative refraction and wave focusing. Philippe et al. [27] developed a tunable acoustic lens in an isotropic elastic plate that exhibits negative refraction over a finite acoustic frequency range. Similarly, Bramhavar et al. [28] investigated negative refraction and wave focusing of elastic waves in a simple mechanical system consisting of a freestanding plate with a step change in thickness. Darabi et al. [29] studied the broadband cloaking of bending waves using a flexural cloaking structure composed of a single material with homogeneous and isotropic layers, demonstrating near-ideal broadband cloaking in thin plates. Tian and Yu [30] conducted numerical and experimental studies, demonstrating the focusing of an A0-mode wavefront onto a desired focal point by altering the effective plate thickness using a plano-concave aspherical lens bonded to the plate. Similarly, Kudela and Ostachowicz [31] showed that a plano-concave aspherical lens, when attached to the plate, can modify the effective plate thickness and focus the A0 mode of Lamb waves. Another innovative approach proposed by the present authors involves the use of an elastic patch to deflect bending waves through wave refraction [32]. Three types of flat elastic patches have been designed and tested, with their performance investigated through numerical and experimental analyses. These studies primarily focus on the technique of refracting bending waves simply by attaching a metal slice to the plate, without requiring indentation or hole processing. In addition to research utilizing discrete variations in thickness, studies have also been conducted to design gradient index (GRIN) elastic lenses by incorporating gradual thickness variations [33–35]. These studies involve calculating the refractive index based on the thickness profile of the structure and using it to predict the refractive path numerically for wave focusing and energy harvesting applications.

In this study, the analysis focuses on the impact of gradient thickness variation by introducing a pyramid-shaped patch with equivalent mass to the previously studied triangular elastic patch. To make preliminary path

predictions, the study employs the ray tracing method and compares its results with numerical simulation and experimental data. Through these analytical and experimental approaches, the study observes the propagation of elastic waves on thin plates and investigates the refraction and reflection phenomena influenced by patch thickness. The investigation particularly examines diverse wave characteristics concerning incident angles, shedding light on the potential application of the findings in shock reduction.

2. Patch Design for Wave Refraction

2.1. Refraction of Bending Waves. When an elastic wave propagates from one solid to another solid, there are four quantities that must be equal on both sides of the boundary: the normal displacement, the tangential displacements, the normal stress, and the tangential stress [25]. In the case of a bending wave incident on a boundary, as shown in Figure 1, the incident wave vibrates in the xy-plane with an incident angle of β_1. The wave reflects at the same angle and refracts at an angle of β_3. The deviation angle with respect to the direction of the incident waves is defined as γ. In an infinite flat plate, bending waves generated by a concentrated transverse force spread out cylindrically from a source point [36]. According to Huygens's principle, at any given moment, the wavefront is the envelope of a series of spherical wavelets spreading out from points on the wavefront at a previous moment. This principle is used to derive the following sine law (Snell's law) relation:

$$\frac{\sin(\beta_1)}{c_A} = \frac{\sin(\beta_2)}{c_A} = \frac{\sin(\beta_3)}{c_B}, \tag{1}$$

where c_A and c_B are the propagation velocities of the bending waves in the first plate and the second plate, respectively. This means that for a given pair of media, the degree to which a wave is refracted is determined by the change in wave speed and the initial direction of the incident wavefronts. The propagation velocity of bending waves, denoted as "c," in a thin and uniform plate is determined using the following equation [36, 37]:

$$c = \sqrt{\omega}\left(\frac{D}{m}\right)^{1/4}, \tag{2}$$

where D represents the bending stiffness of the plate, ω is the phase frequency of bending waves, and m is mass per unit area.

In the analysis of wave refraction and reflection phenomena in a plate assembly, it is necessary to consider the bending stiffness of the structure. Specifically, to analyze the proposed attachment method with elastic patches, the bending stiffness of the layered plate structure was theoretically investigated [32]. The bending stiffness of the plate assembly is derived as follows:

$$D = t_p z_p'^2 C_{11}^p + t_h z_h'^2 C_{11}^h + \frac{t_p^3}{12} C_{11}^p + \frac{t_h^3}{12} C_{11}^h. \tag{3}$$

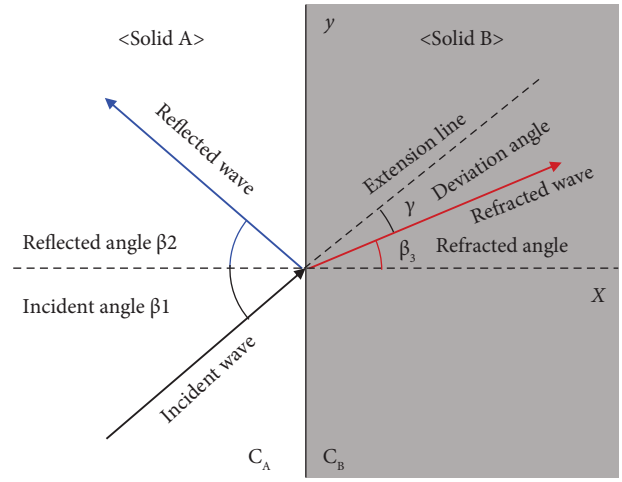

Figure 1: Refraction and reflection behavior of incident waves at the boundary.

The subscripts p and h indicate the patch and host plate respectively. Furthermore, t is the thickness and z' is the location of the neutral axis with respect to the neutral axis of assembly. The following equation (4) indicates the linear relation between normal stress and strain [38].

$$C_{11} = \frac{E}{1-\nu^2}, \tag{4}$$

where E, ν represents the Young's modulus and Poisson ratio, respectively.

Under specific conditions, when the propagating wave passes through a boundary, it undergoes reflection without refraction, which is known as total internal reflection. The angle of incidence that makes β_3 equal to 90 degrees in equation (5) is referred to as the critical angle (β_c), which can be determined using the following equation:

$$\beta_c = \sin^{-1}\frac{c_A}{c_B}. \tag{5}$$

When the incident angle is greater than the critical angle, the wave undergoes total reflection, and this characteristic contributes to favorable shock reduction in the region beyond the boundary.

2.2. Gradient Index with Thickness Variations. To investigate the refractive index and wave velocity resulting from gradual thickness variation, an analysis was conducted on a beam-shaped structure. This analysis encompassed both a beam with discrete thickness variation and a beam with gradual thickness variation. To ensure equal areas for both beams, the maximum thickness of the gradual beam was set to 3t. Using the previously derived equations, bending stiffness and wave velocity were calculated along the x-axis, and the bending stiffness and wave velocity at 1t were denoted as D and C, respectively. Additionally, the refractive index at thickness 1t was taken as the reference refractive index (n_{ref}), enabling the determination of relative refractive indices as well. The relative values corresponding to variations in

thickness are presented in Figure 2. The red line represents values for the stepped beam, with all values being discrete. In contrast, for gradual thickness variation (blue line), it is evident that bending stiffness, wave velocity, and refractive index change progressively along the x-axis. Furthermore, even with the same mass, the maximum values and their deviations are more pronounced. When applied to the patch configuration proposed in this study, continuous refraction of waves within the patch area is expected due to the significant variation in bending wave properties. This suggests that, compared to the flat type, the proposed patch could exhibit greater refraction angles owing to the substantial variability in bending wave properties.

In this study, we experimentally and analytically analyzed the refraction and reflection phenomena of triangular-shaped patches. Two types of patches were fabricated: one with a discrete thickness variation, designed to have flat configuration, and the other with a gradual thickness variation, designed in a pyramid shape. The critical length was fixed at 100 mm, and to analyze the elastic wave propagation characteristics according to the incident angle, different α values of 40, 45, and 50 degrees were used, as depicted in Figure 3. To ensure equal mass between flat type and pyramid type, the height of the flat type was set to 1 mm, while pyramid type was designed to have a maximum height of 3 mm. The maximum height is located at the centroid of the triangular patch. The colormaps depicted in Figure 4 represents the relative bending stiffness and refractive index for each type's half model, respectively. D_{host} and n_{host} denote the bending stiffness and refractive index on a plate with a thickness of 1 mm, and the properties of the structure with the attached patch on the plate were computed. In the case of the pyramid type, a gradient variation in both stiffness and refractive index is observed across the entire patch area, with a notable deviation significantly larger compared to the flat type.

3. Numerical Analysis

3.1. Prediction of Propagation Path with Ray-Tracing Method. To initially assess and compare the propagation characteristics in the rear region of each patch type and incident angle, we employed the ray tracing method, a well-established technique widely used in fields such as ocean acoustics, seismology, and optics. Although ray tracing assumes a straight-line propagation of bending waves through the structure, it does not account for interference and diffraction effect [39]. Nevertheless, this approach remains a valuable tool for predicting the wavefront propagation paths.

The ray tracing algorithm established for this study is illustrated in Figure 5. Within the 2-dimensional thickness field in XY-plane, individual beams depart from the point source and travel straightly in discrete small steps, which are sufficiently small to be negligible compared to the patch's overall length. Each point on the N-th beam is denoted as $P_N(i)$, and the corresponding thickness at that point is represented as $T_{N,i}$. The bending stiffness, D_{bend}, plays a crucial role in adjusting the beam direction during travel. When the thickness at a given step "i" deviates from the thickness at the previous step "$i-1$," the beam's direction is modified by the deviation angle, calculated based on the differences in bending stiffness and phase velocity between the two step points.

Once the calculation of the beam trajectory is completed, point clouds are generated along each beam. To evaluate the density field of these point clouds, we employed the kernel density estimation algorithm. This nonparametric method allows us to identify structures in the data sets without requiring a specific model [40]. For this purpose, the Epanechnikov kernel function [41], represented by equation (6), was utilized as the kernel density function. This function facilitates the prediction of high and low response areas based on the following calculated density:

$$K(u) = \frac{3}{4}\left(1 - u^2\right), \ \{|u| < 1\}. \tag{6}$$

The kernel function, $K(u)$, is the weighting function that is commonly used in nonparametric estimation methods to smooth data by calculating a weighted average of the observed neighboring data. In equation (7), the normalized distance from the selected point to the neighboring data is represented by u, and is defined as follows:

$$u = \frac{\left\| X_P - X \right\|}{R}, \tag{7}$$

where X_p and X are coordinates of the selected point and its neighboring data point, respectively, and R is the radius of the window.

The numerical simulations of triangular elastic patches were carried out using the ray tracing algorithm and kernel density estimation. As shown in Figure 6, the analysis domain encompasses a size of 550 mm × 200 mm. Within this domain, a host plate with a thickness of 1 mm was considered, along with a 0.4 mm thick adhesive layer. Additionally, thickness fields were generated for each individual patch within the domain. The patches were made of aluminum alloy, which was also used for the host plate. The material properties of the aluminum alloy and adhesive (Epoxy resin) are provided in Table 1.

Figure 7 shows the beam trajectories and the normalized density field for triangle flat patches with α of 40 degrees, 45 degrees, and 50 degrees. From the results, it can be observed that for the triangular flat patch with a discrete thickness variation, the critical angle is approximately 45 degrees. When the incident angle exceeds this critical angle ($\alpha = 40$ degrees), total reflection is observed. However, when the incident angle is smaller ($\alpha = 50$ degrees), refraction occurs, and the wave pass through the interior of the patch. The results for the pyramid-shaped patches are presented in Figure 8. In the case of the Pyramid type, due to its gradual thickness variation, the beam's refraction path changes progressively, leading to continuous refraction within the patch. This characteristic results in different refraction behaviors for bending waves with the same incident angle as the flat type. For instance, when α is 40 degrees, similar to the flat type, most of the waves experience total reflection. However, when α is 45 degrees, the flat type exhibits wave

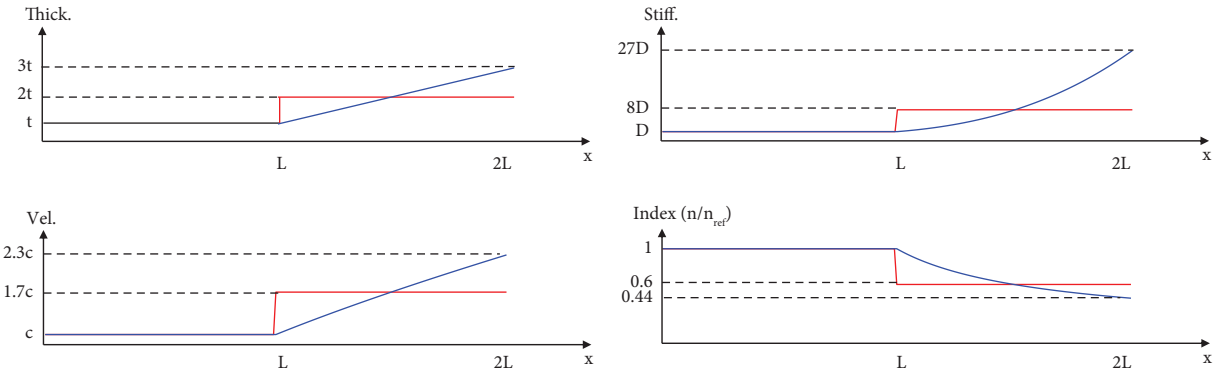

Figure 2: Bending stiffness, wave velocity, and refractive index profile for beams with stepped and gradual thickness variations.

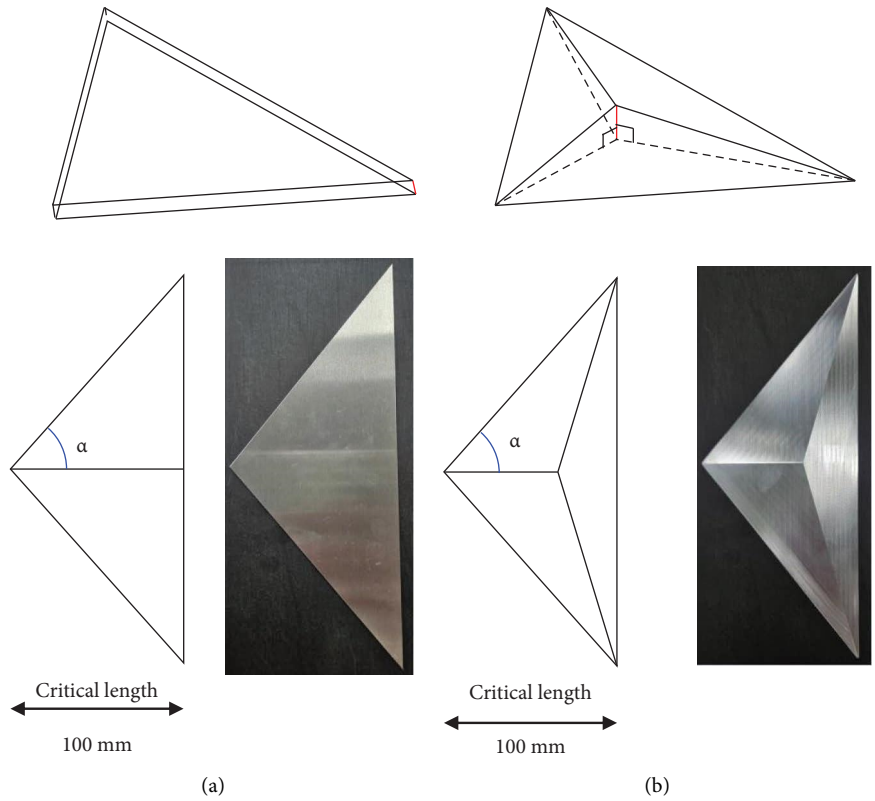

Figure 3: Triangular elastic patches for (a) flat type and (b) pyramid type.

propagation along the boundary, whereas the pyramid type demonstrates a phenomenon akin to total reflection. Furthermore, at the α of 50 degrees, the flat type primarily exhibits refraction, while the pyramid type shows a predominantly reflective response. These results indicate that the gradual thickness variation in the pyramid type induces different refraction behaviors for a broader range of incident angles. By employing such gradual thickness changes, the occurrence of reflective phenomena can be effectively induced at higher incident angles, as confirmed through these findings.

3.2. Finite Element Analysis. Wave propagation on a thin plate can be accurately and effectively simulated through the explicit time integration of the finite element method using the Lagrangian approach [6, 42]. For the numerical simulation of wave propagation in this study, ABAQUS SIMULIA was employed. The finite element model was constructed with symmetric geometry, as shown in Figure 9, utilizing a total 240,000 nodes and 150,000 elements. To account for the adhesive layer between the host plate and the patch, an epoxy layer with a presumed thickness 0.4 mm was included in the model. The host plate, composed of AL-

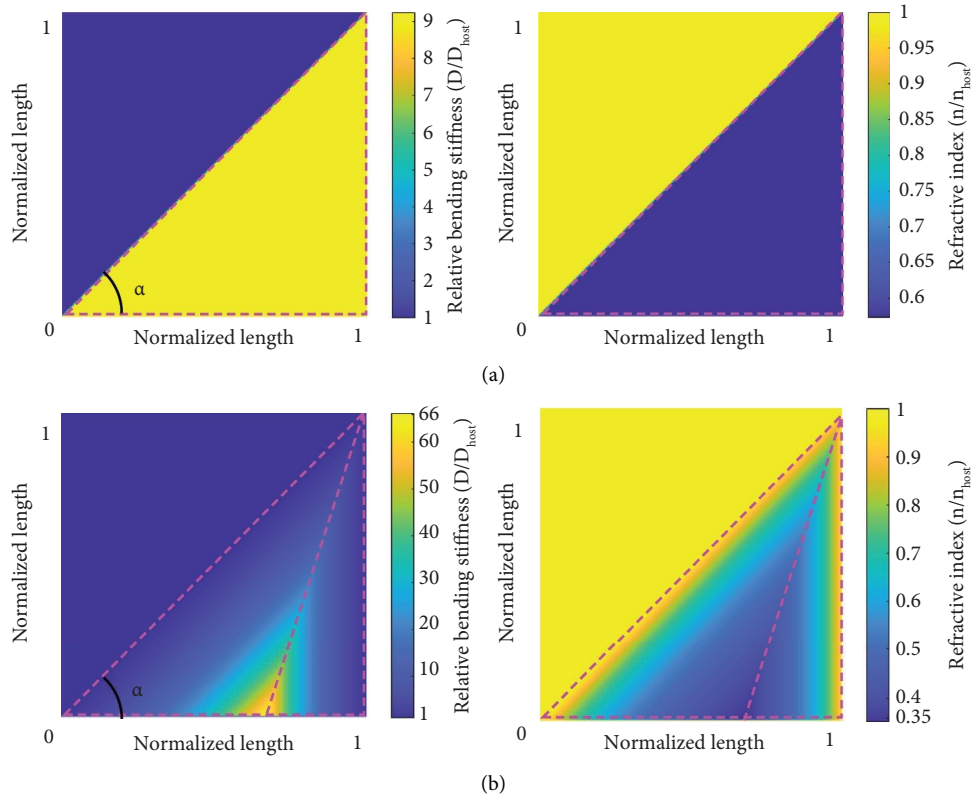

Figure 4: Colormaps of relative bending stiffness and refractive index for (a) flat type and (b) pyramid type.

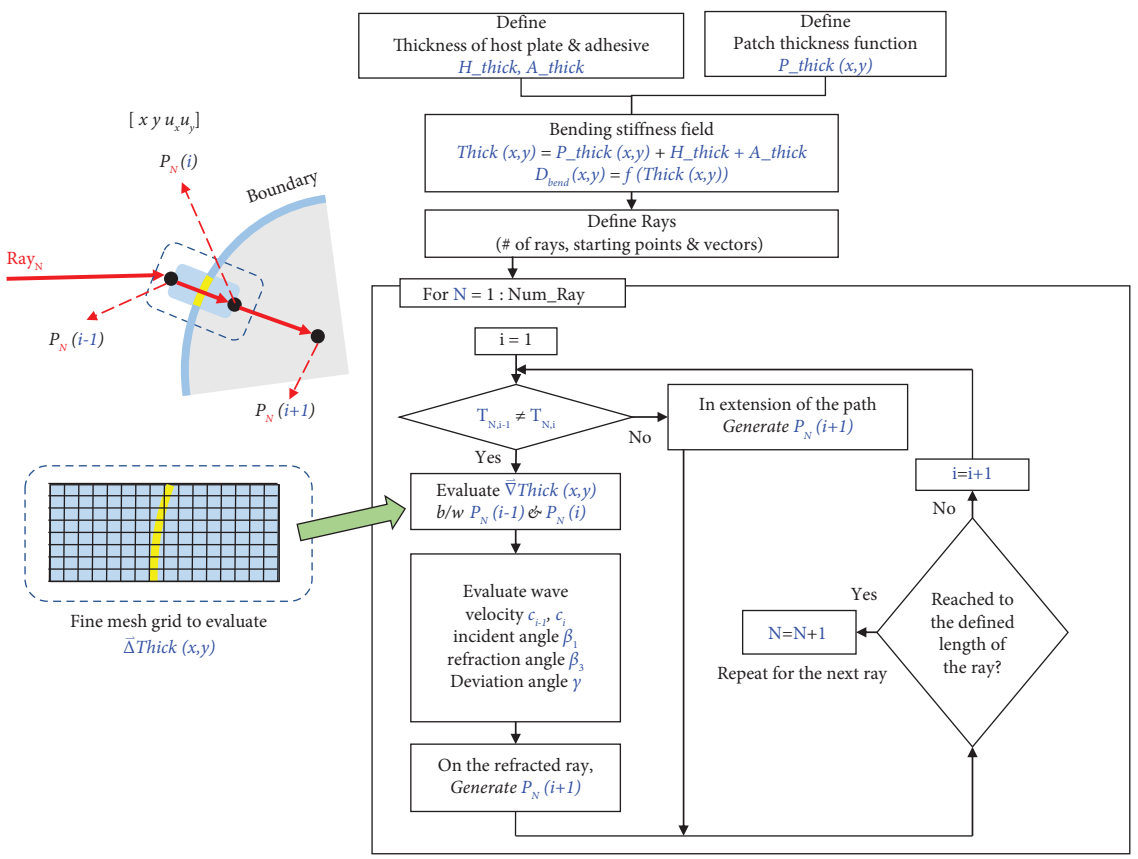

Figure 5: Ray-tracing algorithm for prediction of elastic wave path.

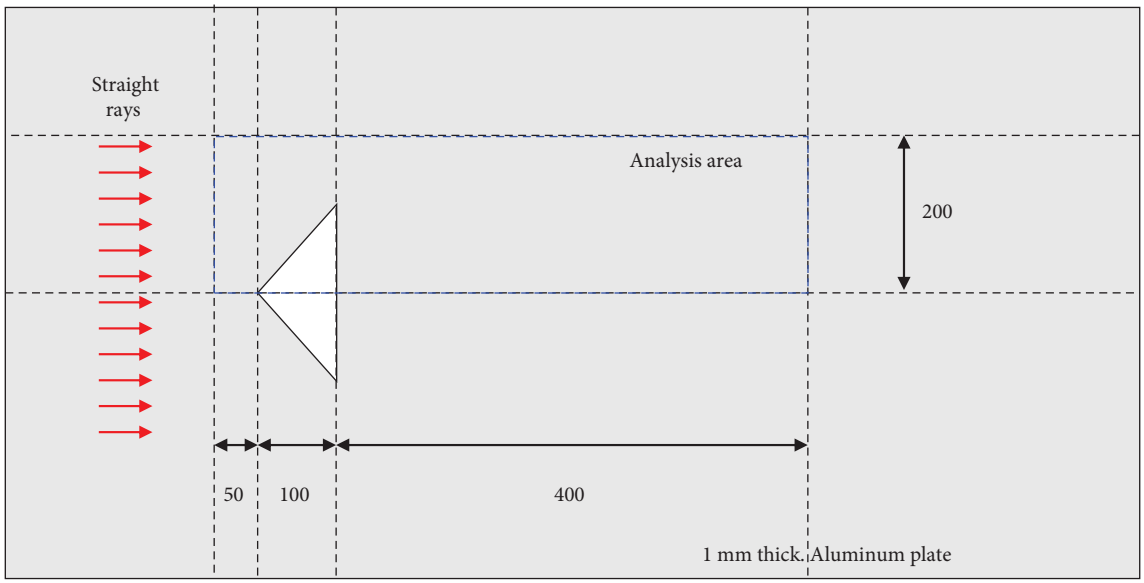

Figure 6: Analytical model of thickness field for ray-tracing analysis.

Table 1: Material properties of aluminum alloy and adhesive [42].

	Density (kg/m^3)	Young's modulus (GPa)	Shear modulus (GPa)	Poisson's ratio
Aluminum	2770	71	26.7	0.3
Epoxy resin	1160	3.78	1.4	0.35

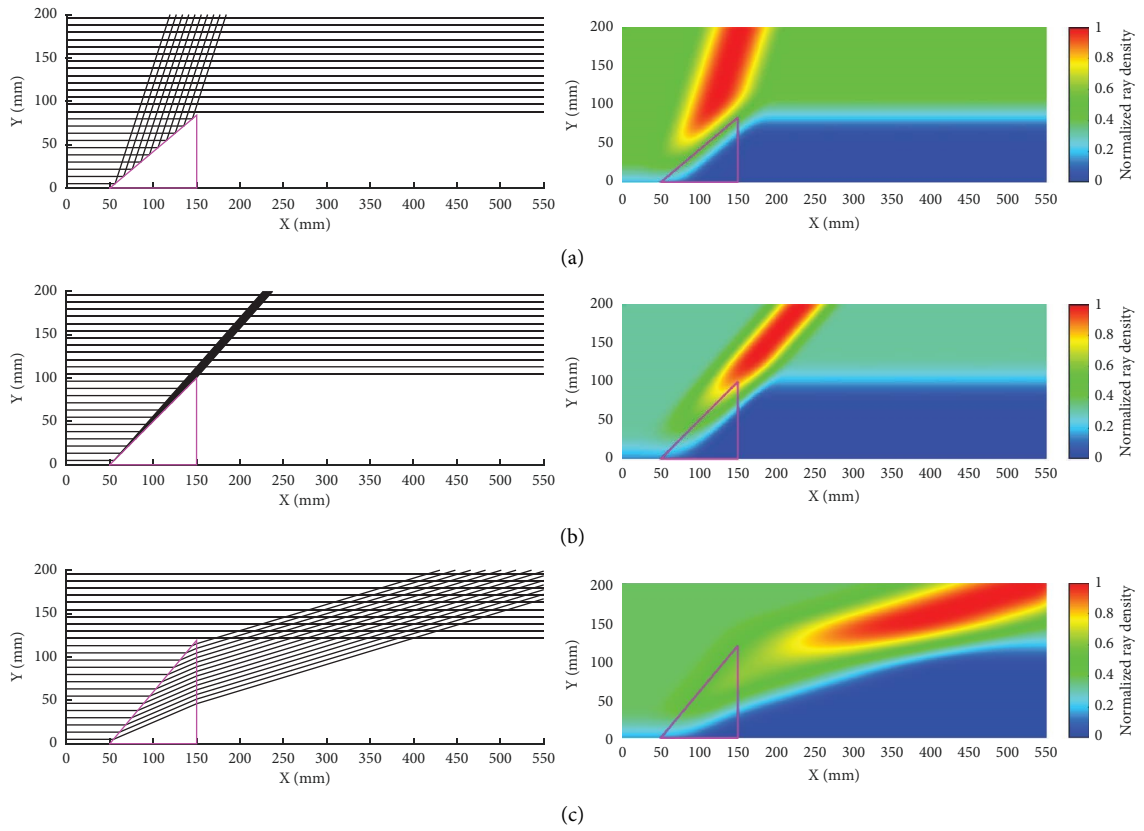

Figure 7: Beam trajectories and the normalized density field for triangle flat patches with α of (a) 40 degrees, (b) 45 degrees, and (c) 50 degrees.

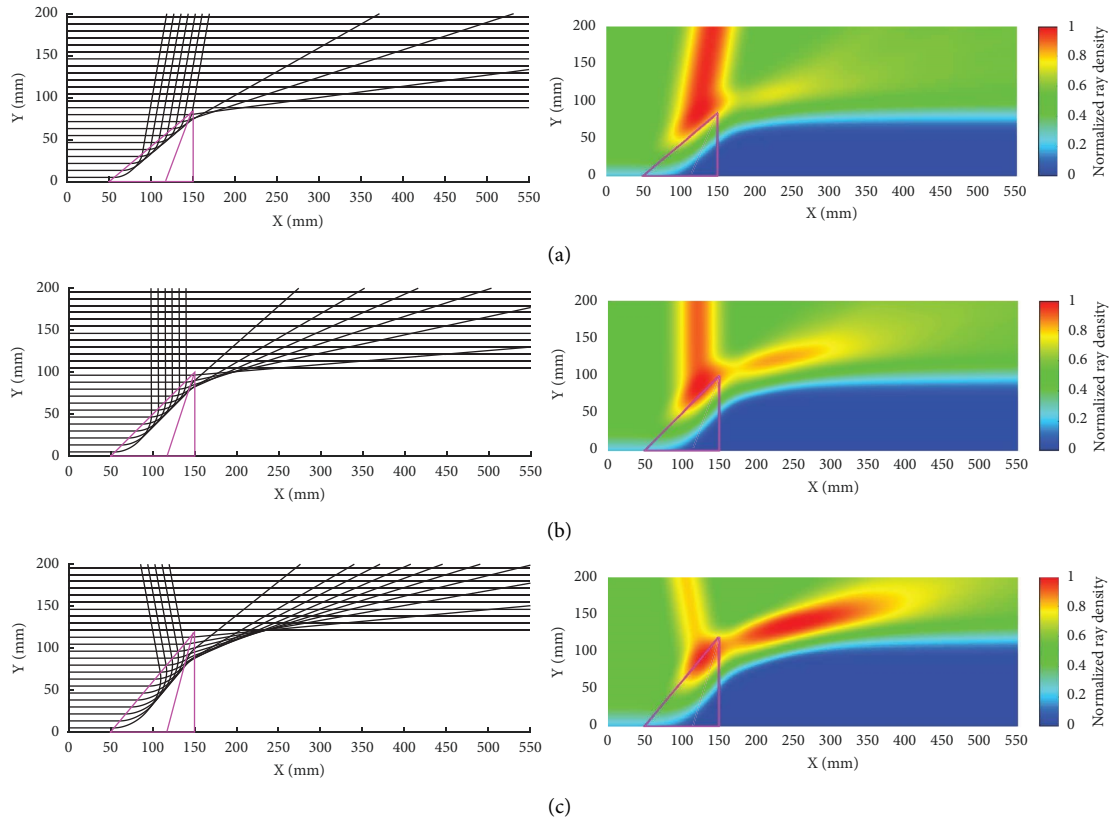

Figure 8: Beam trajectories and the normalized density field for triangle pyramid patches with α of (a) 40 degrees, (b) 45 degrees, and (c) 50 degrees.

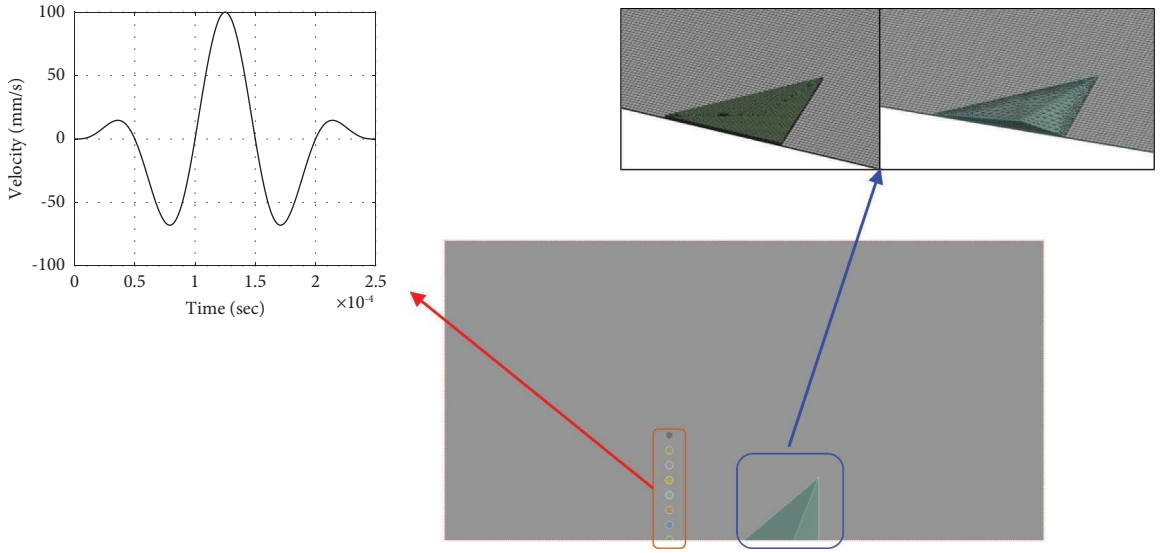

Figure 9: Finite element model for numerical simulations.

6061-T6 with a thickness of 1 mm, shares the same material properties with the elastic patch, which has a right-angled triangle shape in this case. Additionally, 15 thin disks with a thickness of 0.5 mm and a diameter of 10 mm were modeled to replicate piezo actuators. To induce bending wave, a Hanning windowed Z-directional sinusoidal velocity boundary condition with a peak amplitude of 100 mm/s and a frequency of 10 kHz was applied to the disks. Material properties and coefficients of the shock equation of state (EoS) for AL-6061-T6 and epoxy are listed in Table 2. These parameters are crucial for accurately modeling the wave propagation behavior in the numerical simulation.

Table 2: Material properties of AL-6061-T6 and epoxy resin [32].

	AL-6061-T6	Epoxy adhesive
Density (kg/m^3)	2703	1186
Shear modulus (GPa)	27.6	2
Gruneisen coefficient	1.97	1.13
Parameter C_1 (m/s)	5240	2730
Parameter S_1	1.40	1.493
Parameter S_2 (s/m)	0	0

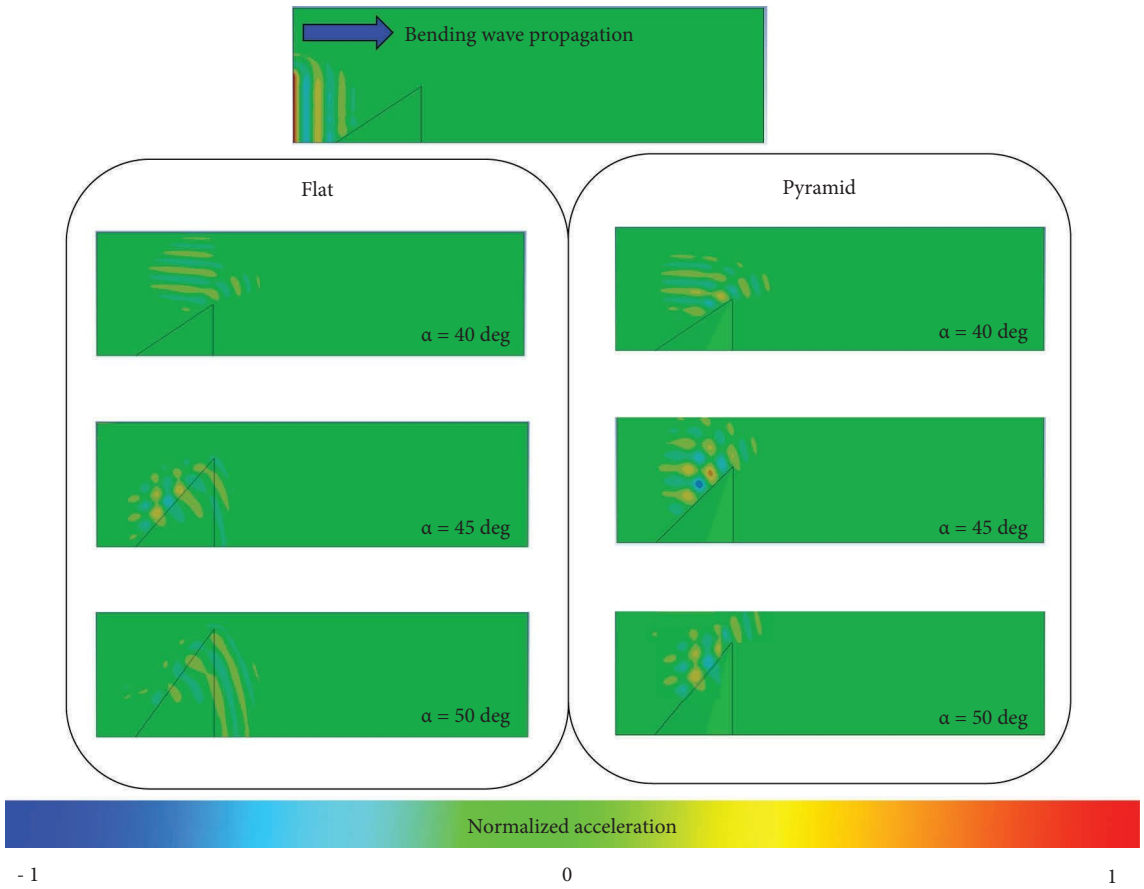

Figure 10: Normalized acceleration wavefield for finite element model at time = 0.7 ms.

The results of the finite element analysis are presented in Figure 10. It is observed that bending waves generated by the disk actuators propagate on the thin plate, and upon encountering the elastic patch, refraction and reflection phenomena are evident. For the flat patch, the numerical results align with the theoretical outcomes. At an α of 40 degrees, total reflection occurs, and at 45 degrees, the critical angle is reached, leading to wave propagation along the boundary. Moreover, at 50 degrees, refraction dominates, and the waves pass through the interior of the patch. On the other hand, for the pyramid type, the numerical results are consistent with the ray tracing algorithm. In all cases, a substantial portion of the energy undergoes reflection, as observed. These findings further confirm that the finite element analysis effectively simulates the propagation of bending waves and accurately captures the refraction and reflection phenomena that occur when these waves encounter the elastic patches.

4. Experimental Analysis

4.1. Experimental Setup. In order to measure and visualize the propagation of elastic waves on a thin plate, a 2-dimensional auto stage scanning system was constructed, as illustrated in Figure 11. The system comprises a laser doppler vibrometer (LDV) installed on a 2-D stage, which measures the out-of-plane velocity response on the patch side. To achieve sufficient and accurate signal measurements, it is crucial to maintain the perpendicular alignment between the laser direction and the plate. In this setup, the host plate is supported and positioned using a wire suspension. For generating elastic waves, a 1-D array of 15

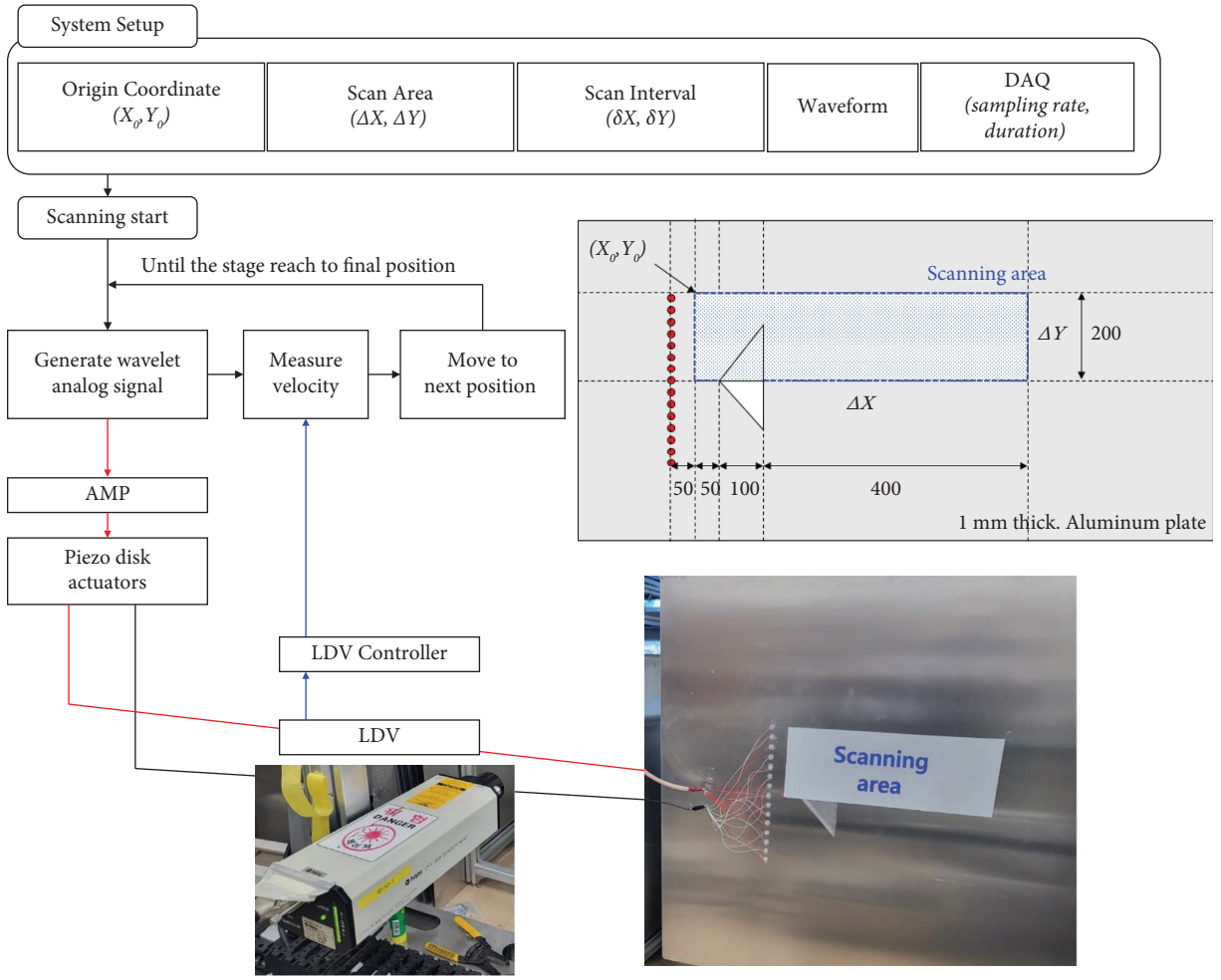

Figure 11: Schematic diagram and configuration of 2-dimensional auto stage scanning system.

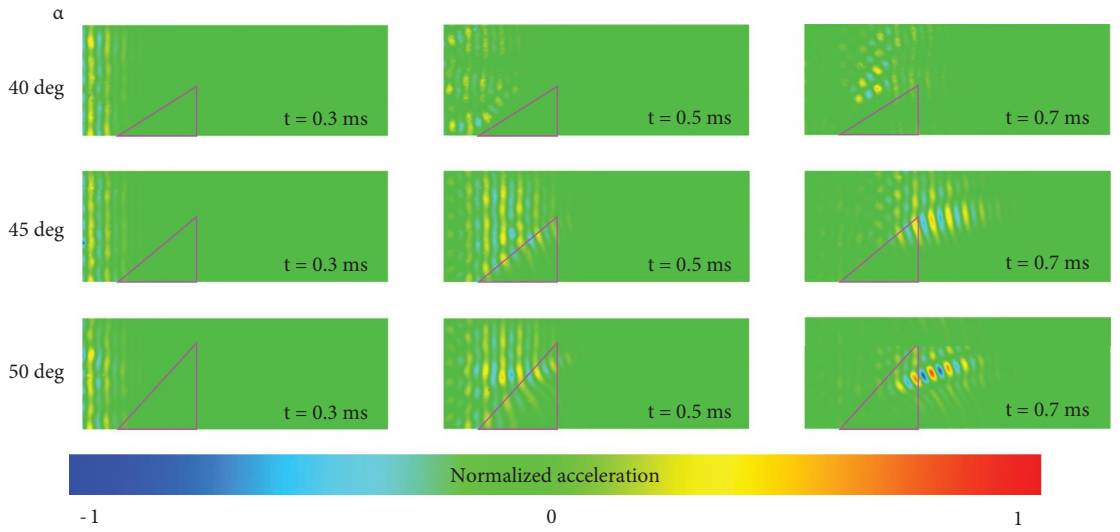

Figure 12: Time-dependent normalized acceleration wavefield for the experimental measurements on the flat type.

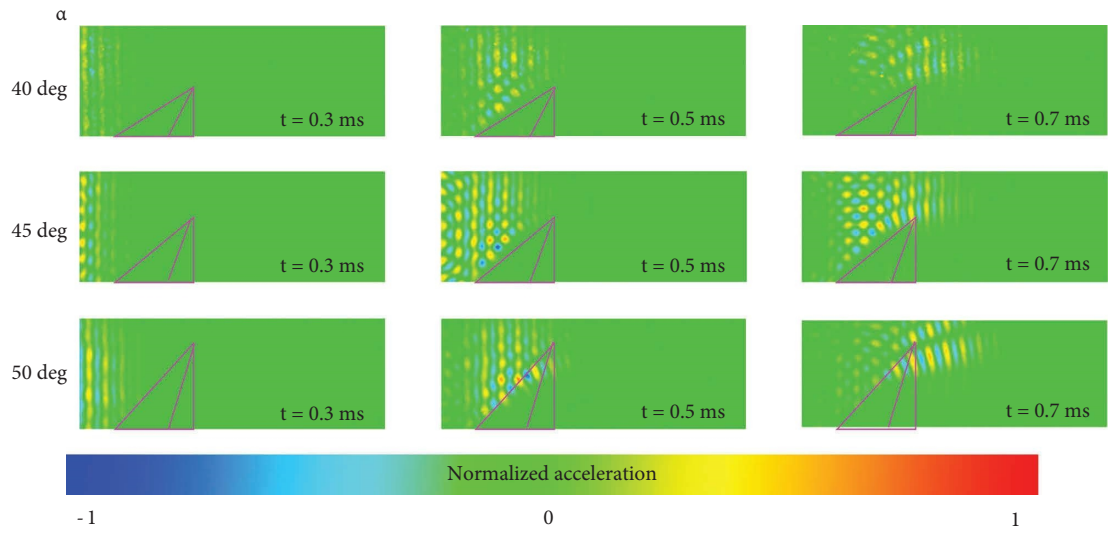

Figure 13: Time-dependent normalized acceleration wavefield for the experimental measurements on the pyramid type.

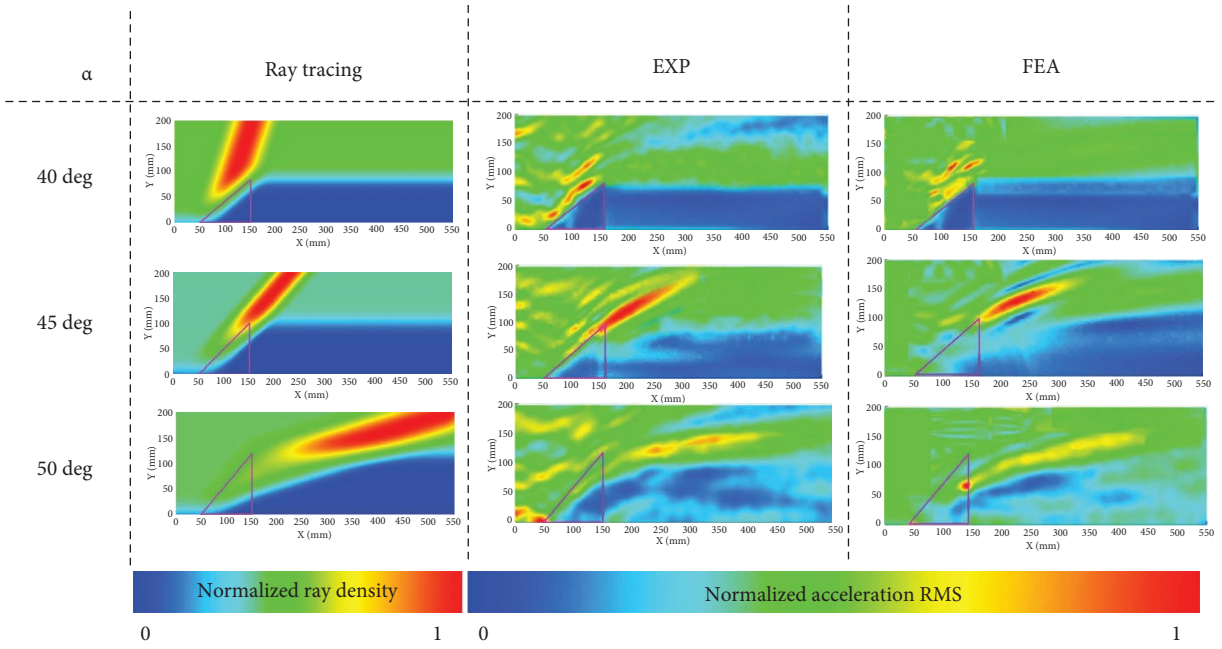

Figure 14: Normalized acceleration RMS fields of experimental and numerical results for flat patch.

piezoelectric disks made of PIC255, a piezoelectric ceramic material, was attached to the host plate. Each disk has a diameter of 10 mm and a thickness of 0.5 mm. The input voltage waveform applied to the piezo disk actuators was a Hanning-windowed sinusoidal signal consisting of three periods, with a voltage amplitude ranging 0 V to 300 V. The signal was amplified using a Trek-623B piezoelectric driver. Velocity data at each sensing point were recorded with a sampling rate of 1 MHz using a National Instruments PXIe-6366 DAQ board. The scanning area was set to 550 mm width × 200 mm height, with 3 mm intervals between each measurement point, resulting in a total of 12,328 points being measured. It is very important that the reflected signal should not interfere the waves at scanning area. We simply employed sufficiently large host plate (1200 mm × 1200 mm) so that all the measurement at scanning area has been completed before the signal reflected at the boundary arrives at the area of interest. In this experiment, the sampling frequency was set to 1 MHz, and the duration of the measurements was 40 ms. The velocity data obtained from the measurements were differentiated to convert them into acceleration values. This scanning system allowed for precise measurements of the wave propagation over the entire scanning area, facilitating the visualization and analysis of the elastic wave behavior on the thin plate.

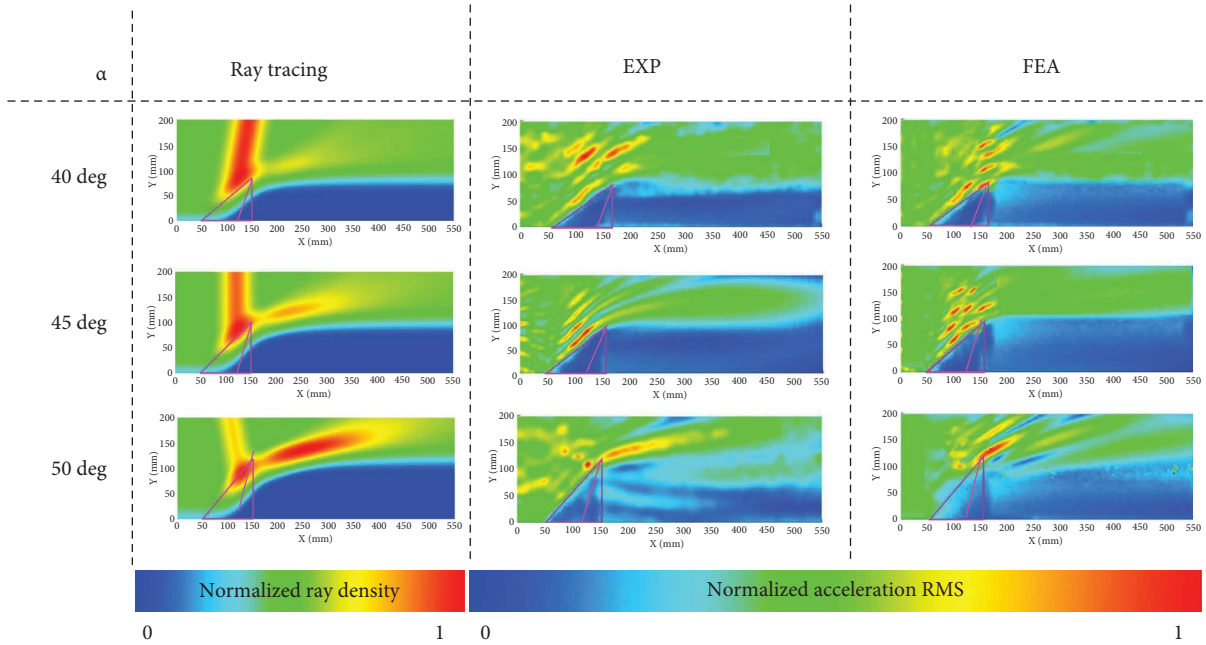

Figure 15: Normalized acceleration RMS fields of experimental and numerical results for pyramid patch.

Table 3: Shock reduction performance.

α (deg)	40		45		50	
Shape	Flat	Pyramid	Flat	Pyramid	Flat	Pyramid
RMS reduction ratio	0.83	0.86	0.47	0.78	0.22	0.71
RMS reduction/patch mass (normalized)	0.96	1	0.56	0.86	0.21	0.69

4.2. Experimental Results. Figure 12 represents the time-dependent normalized acceleration wavefield for the experimental measurements on the flat type. Upon observing the wavefield at 0.3 ms, it is evident that the bending wave is effectively generated by the piezo disk actuators. At 0.5 ms, one can observe the refraction and reflection phenomena caused by the thickness variation, which can be compared with the existing numerical analysis results. The experimental results exhibit excellent agreement with the analytical outcomes, accurately reflecting refraction, reflection, and the critical angle condition, thus confirming the accuracy of the experimental setup. Figure 13 shows the results for the pyramid type, wherein, reflective phenomena dominate in all cases, consistent with the analytical predictions. To quantitatively compare these results with the density field outcomes obtained from the ray tracing method, acceleration-time data at each point were transformed into RMS values. The finite element analysis results and experimental data are compared, as presented in Figures 14 and 15. The similarity between the results generated by the ray tracing method and the experimental data confirms the capability of characterizing wave refraction and reflection phenomena caused by thickness variation. Additionally, it is confirmed that the pyramid type can induce reflective phenomena for a broader range of incident angles compared to the flat type. These results demonstrate the utility of the pyramid type for inducing reflective phenomena over a wider range of incident angles when compared to the flat type. In real shock scenarios, shocks propagate randomly from various directions, unlike the controlled experimental and analytical setups. The utilization of the pyramid type, which can induce reflective phenomena over a wider range of incident angles, could contribute to the improvement in shock reduction performance.

4.3. Shock Reduction Performance. In order to compare the shock reduction performance resulting from the gradual thickness variation, shock reduction values were calculated. This was achieved by comparing the average acceleration RMS values in the prepatch passing region ($0 \le x \le 30$, $0 \le y \le 50$) with those in the postpatch passing region ($170 \le x \le 270$, $0 \le y \le 50$); these areas are indicated in Figure 14. The results are presented in Table 3, including both the shock reduction value and the shock reduction value per patch mass. Upon reviewing the results, it is observed that both types exhibit excellent shock reduction performance in the condition of total reflection ($\alpha = 40$ deg). In this case, the impact of gradual thickness variation appears to be relatively minor. Next, for the critical angle condition ($\alpha = 45$ deg) in the flat type, the pyramid type with reflective phenomena shows superior shock reduction performance. This observation becomes more prominent at $\alpha = 50$ deg, where significant energy reaches the postpatch passing region in the

flat type due to refraction occurring within the patch. On the other hand, for the pyramid type with its design for gradual refraction and reflective effects, improved shock reduction performance is demonstrated. These results indicate that the pyramid type enhances the shock reduction performance, particularly when compared to the flat type in conditions of critical angle and small incident angles, where reflective phenomena are predominant.

5. Conclusion

Reducing structural shocks propagated as elastic waves in thin plate-like structures holds significant importance in various engineering applications. In a previous study, the present authors proposed a shock reduction method utilizing elastic patches, which deflect bending waves through wave refraction without compromising structural stiffness and strength. To further advance this concept, we designed elastic patches with gradually varying thickness and conducted a thorough investigation of their propagation characteristics, both numerically and experimentally. Two types of triangular elastic patches, flat and pyramid-shaped, were employed to refract and reduce transient bending waves at different incident angles. To predict the propagation characteristics, we established ray tracing and density estimation algorithms. The numerical results showcased the distinct propagation behaviors of elastic patches with varying shapes and incident angles. Additionally, finite element analysis was carried out to simulate elastic wave propagation, including refraction and reflection phenomena, on thin plates with elastic patches. To validate and compare these numerical findings with the preliminary ray tracing analysis, we conducted an experimental study using a 2-dimensional auto stage scanning system. The experimental results were presented through visualizations of elastic wave propagation and the normalized RMS value of the acceleration wavefields. Remarkably, all the results from ray tracing, finite element analysis, and experiment consistently demonstrated that the attached patches effectively reduce passing waves in the areas behind the patches. Furthermore, the impact of gradual thickness variation was thoroughly discussed. These findings establish the superiority of the pyramid type in inducing reflective phenomena over a broader range of incident angles compared to the flat type. This characteristic has the potential to enhance shock reduction performance, especially in real scenarios where shocks propagate randomly from various directions, unlike the controlled experimental and analytical setups. In conclusion, our proposed method offers a practical approach to mitigating transient shock responses in specific target areas across various structural applications, without compromising structural stiffness and strength. Through the straightforward application of an elastic patch, sensitive components can be effectively safeguarded.

Data Availability

The visual illustration data used to support the findings of this study are included in the article.

Conflicts of Interest

The authors declare that they have no conflicts of interest regarding the publication of this paper.

Acknowledgments

This work was supported by the National Research Foundation of Korea (NRF) grant funded by the Korea government (MSIT) (no. NRF-2021R1A2C2004563) and the BK21 FOUR program of the National Research Foundation Korea (NRF) grant funded by the Ministry of Education (MOE).

References

[1] M. Yu, X. Gao, and Q. Chen, "Study of the mechanical properties and vibration isolation performance of a molecular spring isolator," *Shock and Vibration*, vol. 2016, Article ID 6451829, 10 pages, 2016.

[2] I. Kovacic, M. J. Brennan, and T. P. Waters, "A study of a nonlinear vibration isolator with a quasi-zero stiffness characteristic," *Journal of Sound and Vibration*, vol. 315, no. 3, pp. 700–711, 2008.

[3] S.-H. Youn, Y.-S. Jang, and J.-H. Han, "Development of a three-axis hybrid mesh isolator using the pseudoelasticity of a shape memory alloy," *Smart Materials and Structures*, vol. 20, no. 7, 75112 pages, 2011.

[4] H.-K. Jeong, J.-H. Han, S.-H. Youn, and J. Lee, "Frequency tunable vibration and shock isolator using shape memory alloy wire actuator," *Journal of Intelligent Material Systems and Structures*, vol. 25, no. 7, pp. 908–919, 2014.

[5] H.-K. Jeong, J. Lee, J.-H. Han, and N. M. Wereley, "Design of frequency-tunable mesh washer isolators using shape memory alloy actuators," *Journal of Intelligent Material Systems and Structures*, vol. 27, no. 9, pp. 1265–1280, 2016.

[6] H.-S. Park, D.-H. Hwang, J.-H. Han, and J. Yang, "Development of shock-absorbing insert for honeycomb sandwich panel," *Aerospace Science and Technology*, vol. 104, Article ID 105930, 2020.

[7] Z. Ba, M. Wu, and J. Liang, "3D dynamic responses of a multilayered transversely isotropic saturated half-space under concentrated forces and pore pressure," *Applied Mathematical Modelling*, vol. 80, pp. 859–878, 2020.

[8] J. Liang, M. Wu, and Z. Ba, "Simulating elastic wave propagation in 3-D layered transversely isotropic half-space using a special IBEM: hill topography as an example," *Engineering Analysis with Boundary Elements*, vol. 124, pp. 64–81, 2021.

[9] M. Wu, B. Wang, Z. Ba, K. Dai, and J. Liang, "Vibration isolation of infinitely periodic pile barriers for anti-plane shear waves: an exact series solution," *Soil Dynamics and Earthquake Engineering*, vol. 176, Article ID 108347, 2024.

[10] C. Coulais, D. Sounas, and A. Alu, "Static non-reciprocity in mechanical metamaterials," *Nature*, vol. 542, no. 7642, pp. 461–464, 2017.

[11] R. Zhu, X. Liu, G. Hu, C. Sun, and G. Huang, "Negative refraction of elastic waves at the deep-subwavelength scale in a single-phase metamaterial," *Nature Communications*, vol. 5, no. 1, p. 5510, 2014.

[12] B. Li, K. Deng, and H. Zhao, "Acoustic guiding and subwavelength imaging with sharp bending by sonic crystal," *Applied Physics Letters*, vol. 99, no. 5, Article ID 051908, 2011.

[13] H. Huang, Z. Tan, S. Huo, L. Feng, J. Chen, and X. Han, "Topologically protected zero refraction of elastic waves in pseudospin-Hall phononic crystals," *Communications Physics*, vol. 3, no. 1, p. 46, 2020.

[14] Y.-K. Ahn, H.-J. Lee, and Y.-Y. Kim, "Conical refraction of elastic waves by anisotropic metamaterials and application for parallel translation of elastic waves," *Scientific Reports*, vol. 7, no. 1, Article ID 10072, 2017.

[15] S. Li, J. Xu, and J. Tang, "Tunable modulation of refracted lamb wave front facilitated by adaptive elastic metasurfaces," *Applied Physics Letters*, vol. 112, no. 2, Article ID 021903, 2018.

[16] X. Yan, R. Zhu, G. Huang, and F. G. Yuan, "Focusing guided waves using surface bonded elastic metamaterials," *Applied Physics Letters*, vol. 103, no. 12, Article ID 121901, 2013.

[17] S. Tol, F. L. Degertekin, and A. Erturk, "Phononic crystal Luneburg lens for omnidirectional elastic wave focusing and energy harvesting," *Applied Physics Letters*, vol. 111, no. 1, Article ID 013503, 2017.

[18] S. Tol, F. L. Degertekin, and A. Erturk, "3D-printed phononic crystal lens for elastic wave focusing and energy harvesting," *Additive Manufacturing*, vol. 29, Article ID 100780, 2019.

[19] V. V. Krylov and F. J. B. S. Tilman, "Acoustic 'black holes' for flexural waves as effective vibration dampers," *Journal of Sound and Vibration*, vol. 274, no. 3-5, pp. 605–619, 2004.

[20] D. O'Boy and V. Krylov, "Damping of flexural vibrations in circular plates with tapered central holes," *Journal of Sound and Vibration*, vol. 330, no. 10, pp. 2220–2236, 2011.

[21] L. Tang and L. Cheng, "Enhanced acoustic black hole effect in beams with a modified thickness profile and extended platform," *Journal of Sound and Vibration*, vol. 391, pp. 116–126, 2017.

[22] L. Zhao and F. Semperlotti, "Embedded acoustic black holes for semi-passive broadband vibration attenuation in thin-walled structures," *Journal of Sound and Vibration*, vol. 388, pp. 42–52, 2017.

[23] L. Ma, S. Zhang, and L. Cheng, "A 2D Daubechies wavelet model on the vibration of rectangular plates containing strip indentations with a parabolic thickness profile," *Journal of Sound and Vibration*, vol. 429, pp. 130–146, 2018.

[24] H. Ji, X. Wang, J. Qiu, L. Cheng, Y. Wu, and C. Zhang, "Noise reduction inside a cavity coupled to a flexible plate with embedded 2-D acoustic black holes," *Journal of Sound and Vibration*, vol. 455, pp. 324–338, 2019.

[25] H. Kolsky, *Stress Waves in Solids*, Dover Publications, New York, NY, USA, 2012.

[26] J. Pujol, *Elastic Wave Propagation and Generation in Seismology*, Cambridge University Press, Cambridge, UK, 2003.

[27] F. D. Philippe, T. W. Murray, and C. Prada, "Focusing on plates: controlling guided waves using negative refraction," *Scientific Reports*, vol. 5, no. 1, Article ID 11112, 2015.

[28] S. Bramhavar, C. Prada, A. A. Maznev, A. G. Every, T. B. Norris, and T. W. Murray, "Negative refraction and focusing of elastic Lamb waves at an interface," *Physical Review B*, vol. 83, no. 1, Article ID 014106, 2011.

[29] A. Darabi, A. Zareei, M. R. Alam, and M. J. Leamy, "Broadband bending of flexural waves: acoustic shapes and patterns," *Scientific Reports*, vol. 8, no. 1, Article ID 11219, 2018.

[30] Z. Tian and L. Yu, "Wavefront modulation and controlling for Lamb waves using surface bonded slice lenses," *Journal of Applied Physics*, vol. 122, no. 23, 2017.

[31] P. Kudela and W. Ostachowicz, "Comparison of Lamb wave focusing performance using wave dispersion-compensated actuation and plano-concave lenses," *Journal of Applied Physics*, vol. 124, no. 9, Article ID 094901, 2018.

[32] D.-H. Hwang and J.-H. Han, "Shock reduction technique on thin plate structure by wave refraction using an elastic patch," *Shock and Vibration*, vol. 2021, Article ID 6836899, 14 pages, 2021.

[33] D. Lee, Y. Hao, J. Park et al., "Singular lenses for flexural waves on elastic thin curved plates," *Physical Review Applied*, vol. 15, no. 3, Article ID 034039, 2021.

[34] A. Climente, D. Torrent, and J. Sánchez-Dehesa, "Gradient index lenses for flexural waves based on thickness variations," *Applied Physics Letters*, vol. 105, no. 6, Article ID 064101, 2014.

[35] A. Zareei, A. Darabi, M. J. Leamy, and M.-R. Alam, "Continuous profile flexural GRIN lens: focusing and harvesting flexural waves," *Applied Physics Letters*, vol. 112, no. 2, Article ID 023901, 2018.

[36] F. J. Fahy, *Foundations of Engineering Acoustics*, Elsevier Academic Press, London, UK, 2000.

[37] K. F. Graff, *Wave Motion in Elastic Solids*, Dover Publications, New York, NY, USA, 1991.

[38] D. Zenkert, *An Introduction to sandwich Structures*, Chameleon Press, London, UK, 1995.

[39] A. Andersen and A. Kak, "Digital ray tracing in two-dimensional refractive fields," *Journal of the Acoustical Society of America*, vol. 72, no. 5, pp. 1593–1606, 1982.

[40] M. P. Wand and M. C. Jones, *Kernel Smoothing*, CRC Press, Boca Raton, FL, USA, 1994.

[41] V. A. Epanechnikov, "Non-parametric estimation of a multivariate probability density," *Theory of Probability and Its Applications*, vol. 14, no. 1, pp. 153–158, 1969.

[42] A. Prakash, J. Rajasankar, N. Anandavalli, M. Verma, and N. R. Iyer, "Influence of adhesive thickness on high velocity impact performance of ceramic/metal composite targets," *International Journal of Adhesion and Adhesives*, vol. 41, pp. 186–197, 2013.